# Energy materials

CrossMark

# Molybdenum oxide 2-D flakes: role of thickness and annealing treatment on the optoelectronic properties of the material

A. Domínguez[1], A. Dutt[1] , O. de Melo[2] , L. Huerta[1], and G. Santana[1,*]

[1] *Departamento de Materiales de Baja Dimensionalidad, Instituto de Investigaciones en Materiales, UNAM, Circuito Exterior s/n, C.U., A. P. 70-360, Coyoacán, Ciudad de México 04510, Mexico*
[2] *Physics Faculty, University of Havana, 10400 Habana, La Habana, Cuba*

## ABSTRACT

Molybdenum oxide ($MoO_x$) thin films were grown by using a simple, economic and scalable DC Cressington sputtering unit. For thickness measurement with the quartz balance, during the deposition, $MoO_x$ density was set to an average value of $5.58$ g/cm$^3$ which is the mean density of the two main oxidation states, $MoO_2$ ($6.47$ g/cm$^3$) and $MoO_3$, ($4.69$ g/cm$^3$), respectively. Afterward, as-deposited samples were annealed in air at 400 °C for 60 min. Then onwards, X-ray diffraction (XRD), field emission scanning microscopy, atomic force microscopy (AFM), UV–visible (UV–Vis) spectroscopy and photoconductivity studies were carried out to investigate the differences appearing in the structural, morphological and optoelectronic properties of the as-deposited and annealed samples. Using AFM and SEM, it was observed a decrease in the average roughness as well in the grain size for thicker samples (after annealing), whereas contrary behavior was found for thinner samples. Presence of $\alpha$-$MoO_3$ and sub-oxide phases such as $\beta$-$MoO_2$ and $\gamma$-$Mo_4O_{11}$ with predominance of $MoO_2$ was observed before annealing. XRD and XPS analysis revealed a better crystalline structure for annealed samples in which the $MoO_3$ phase was observed in majority. Depending on the thickness and oxidation states, the electrical behavior of the samples was found to be varied from semimetal to semiconductor. After annealing, all samples shown a semiconductor behavior, with an increase in photoconductivity response for the films with a lower band gap. The aim of the present work is to provide useful information over the control of the morphology and functionality of the thin films with a view to their use for future prospective application especially for the fabrication of hole transport layer in the new generation of solar cells.

Address correspondence to E-mail: gsantana@iim.unam.mx

Springer

## Introduction

Transition metal oxides (TMOs) are very interesting materials because of their technological applications in various fields such as optical smart windows, electrochromic display devices and gas sensors [1–3]. To the TMOs family belongs titanium, manganese, tungsten, zinc, copper, vanadium, cobalt, rhodium and molybdenum oxides, which exhibit a wide range of electronic properties ranging from insulating to semiconducting and conducting behavior. Most interestingly, their properties could be easily engineered by changing their deposition conditions, morphology and stoichiometry [4].

Among the various TMOs, molybdenum oxides ($MoO_x$) have shown interesting structural, optical and chemical properties. Because of their suitable memory and chromogenic properties, they can be used in solid-state batteries, as well in electronic display devices. Most importantly, because of their high work function, they have been used as back surface field in modern solar cells [5–7]. Additionally, carrier selectivity along with the asymmetry in conductivity has also established sub-stoichiometric molybdenum oxide $MoO_x$ ($x < 3$) as a charge selective contact layers [8–10]. Preferential conductivity for one kind of charge carrier (i.e., holes) while blocking the other kind (electrons) helps in the split-up of photo-generated carriers which is extensively used for fabrication of special contacts in the modern solar cells [10–13]. It has also been recently shown that when these films are thermally evaporated, they can provide good surface passivation to c-Si [13].

In general, molybdenum oxides have a wide band gap of 2.8–3.6 eV and a layered structure, with a very special 2D morphology. In a previous report, a very nice description about the laminar structural parameters of $MoO_x$ thin films is given [14]. $MoO_2$ and $MoO_3$ phases can coexist with sub-oxides ($Mo_nO_{3n-1}$) [15]. It has been found earlier that when the $MoO_3$ (010) surface is exposed to the electron or ion beams, it could reduce the surface and forms $Mo_nO_{3n-1}$ species; this effect is correlated with oxygen loss from the structure [15–18]. Furthermore, it has been found that whenever there is a reduction in the oxidation state, a defect band below the conduction band is formed which results in semimetallic character of the films [10]. Additionally, it has been reported that variation in oxygen concentration induces modifications in the interatomic distance [14, 19]. Also, as depicted earlier by Chen et al. [20] oxygen vacancies play an important role in modifying the electronic and the optical properties of $MoO_x$ thin films. In addition, it has been reported earlier that a variation could occur in the conductivity of molybdenum oxides thin films when the transformation occurs from an insulator to semimetallic state [10, 21–24]. As presented in one of the latest reviews, varying the oxidation state could likewise help in tuning the band gap and at the same time could surpass the disadvantage of low carrier concentration of $MoO_3$ thin films, which will make them adequate for the fabrication of electronic devices [25].

$MoO_x$ thin films have been fabricated by different techniques such as sputtering, pulsed laser ablation, electrodeposition, thermal evaporation, spray pyrolysis and sol–gel method among others [26–32]. RF sputtering is generally the preferred technique for the growth of molybdenum oxide thin films. Nevertheless, in case of sputtering unit for the growth of $MoO_x$ thin films, a very high RF power (150 W) and high substrate temperature ($\geq 300\,°C$) are required [33, 34]. Even using these specific deposition conditions, as reported in most of the cases it could result in the formation of amorphous thin films. However, using a simple DC sputtering at a lower substrate temperature, the formation of $MoO_x$ thin films has not been studied extensively. This technique has the advantage of being economic (without the need of high vacuum) and simple in operation. At the same time, it also provides the scalability in the production of high crystalline quality thin films with controlled stoichiometry. These properties make it very suitable for their use in bulk production of devices such as solar cells. Moreover, until a date, control over the optoelectronic properties of $MoO_x$ thin films as in function to their thickness along with the control over the oxidation state has not been reported using a DC sputtering technique.

In this article it is explored, for the first time, the formation of $MoO_x$ thin films grown with a DC sputtering with different thicknesses and oxidation states at low substrate temperature. The effect of annealings carried out on the as-deposited samples of various thicknesses revealed their role for changing the crystallographic structure, chemical composition, morphology and optical properties. The information regarding the phase stability and phase transformation of $MoO_x$ could be very important for practical

implementation of this material in different applications. Finally, change in material type (semimetal and semiconductor behavior) and influence of the oxygen concentration on the band gap have been reported. Foremost, in the present work, photoconductivity of the $MoO_x$ thin films has been studied as in response to the variation in their morphology. Results demonstrated in the present work could provide an insight over the important features and control over the properties of $MoO_x$ thin films for their use in modern generation of solar cells.

## Experimental

### Preparation of molybdenum oxide thin films

Deposition of thin films of $MoO_x$ onto glass and silicon substrates was carried out using a Cressignton DC sputtering unit in Ar atmosphere, at a pressure of 0.1 mbar, a current of 40 mA and a target to substrate distance of 4 cm. Metallic molybdenum (99.95%) was used as a sputter target. Afterward, for detailed studies, annealing in air was carried out at 400 °C for 60 min. Finally, a comparison was carried out between the as-deposited and annealed samples.

It is important to mention here that, for measuring the thickness with the quartz balance, the density of the target was set to 5.58 $g/cm^3$ which is the mean value of the density of $MoO_2$ (6.47 $g/cm^3$) and $MoO_3$ (4.69 $g/cm^3$). This supposition was based on the observation of previous numerous experiments which show that the Mo thin films were always oxidized during growth with mainly those two oxidation states. Further, depending on the quartz balance measured thickness, the samples were classified into four different groups: H1, H2, H3 and H4 with thickness of 90, 180, 270 and 360 nm (measurement by quartz balance), respectively.

### Characterization

For structural characterization, X-ray diffraction (XRD) RIGAKU Ultima IV equipment using a copper (Cu) anode with Kα line of 1.5418 Å was used. Morphological properties were studied using a field emission scanning electron microscopy (FESEM) in a JEOL JSM-7600F equipped with a Schottky emitter electron source. Optical properties were studied from the absorption spectrum by a Filmetrics brand model F10-RT-UV and using the Tauc model, and the film thicknesses were obtained by profilometry and were cross-checked by cross-section micrographs from scanning electron microscopy (SEM). X-ray photoelectron spectroscopy (XPS) analyses were performed in an ultra-high vacuum (UHV) system VG-Scientific Microtech Multilab ESCA2000, with a Mg K_X-ray source (hν = 1486.6 eV), and a CLAM4 MCD analyzer. Dark conductivity and illuminated conductivity were measured using a Keithley 617 programmable electrometer on planar geometry using an illumination system with an equivalent intensity of 100 $mW/cm^2$ and with a similar spectrum of the solar spectrum.

## Results and discussions

Figure 1 shows a comparison of the surface topography of as-deposited (top images) and annealed (bottom images) $MoO_x$ films on Si (100) substrates recorded by atomic force microscopy. Figure 1a–d shows the comparison of four different samples termed as H1, H2, H3 and H4. The AFM image of as-deposited MoOx thin films revealed that the average roughness of the thin films ranges from 9.5 to 17 nm and, for the annealed samples, between 40 and 80 nm. Another remarkable fact could be noted is that the roughness decreases with thickness.

Figure 2 shows the scanning electron microscopy (SEM) images of the as-deposited thin films (H1–H4). Results demonstrated here go well in constancy with the thickness values obtained from the quartz balance in the sputtering system and confirm our supposition that the Mo thin films were oxidized during growth with different mixed oxide phases. For the samples with higher thickness, some variation/reduction could be found which could be correlated with the deposition parameters. As well, results also shown good correlation with the AFM images displayed in Fig. 1. In addition, uniform growth of spherical grains with cracks in the boundaries could be seen in all cases.

However, vast differences in the morphology of the samples were observed due to the annealing and SEM micrographs (Fig. 3c, d) showed the formation of flake (2-D) structure, whereas another interesting fact observed was the increase in the thickness of the annealed samples in comparison with the as-deposited ones. For sample H1, the thickness was
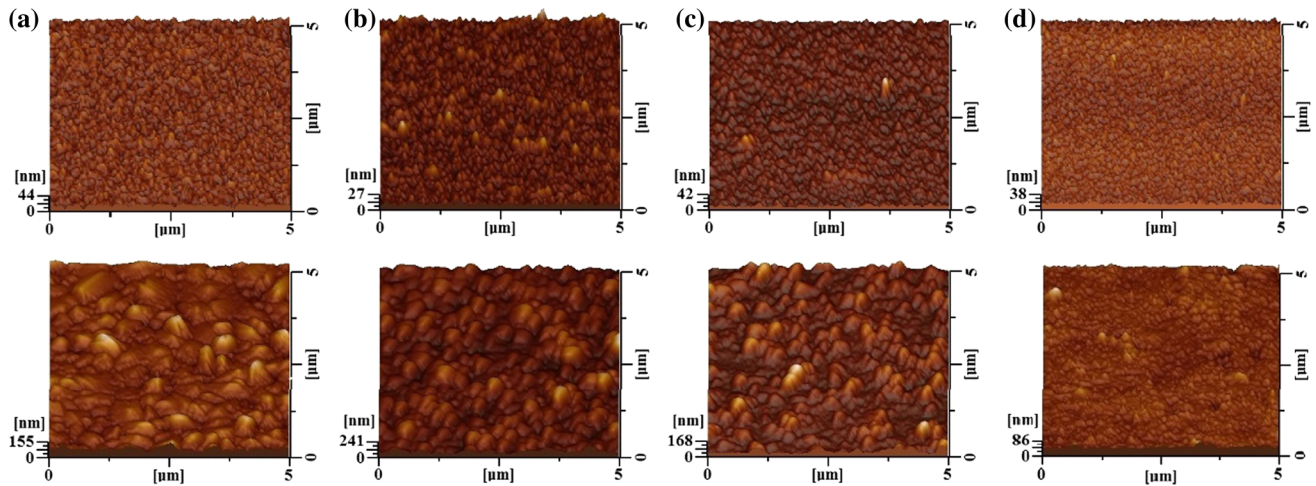
**Figure 1** Topography comparison of the as-deposited (top) and annealed (bottom) $MoO_x$ thin films using AFM analysis: **a** H1, **b** H2, **c** H3 and **d** H4.
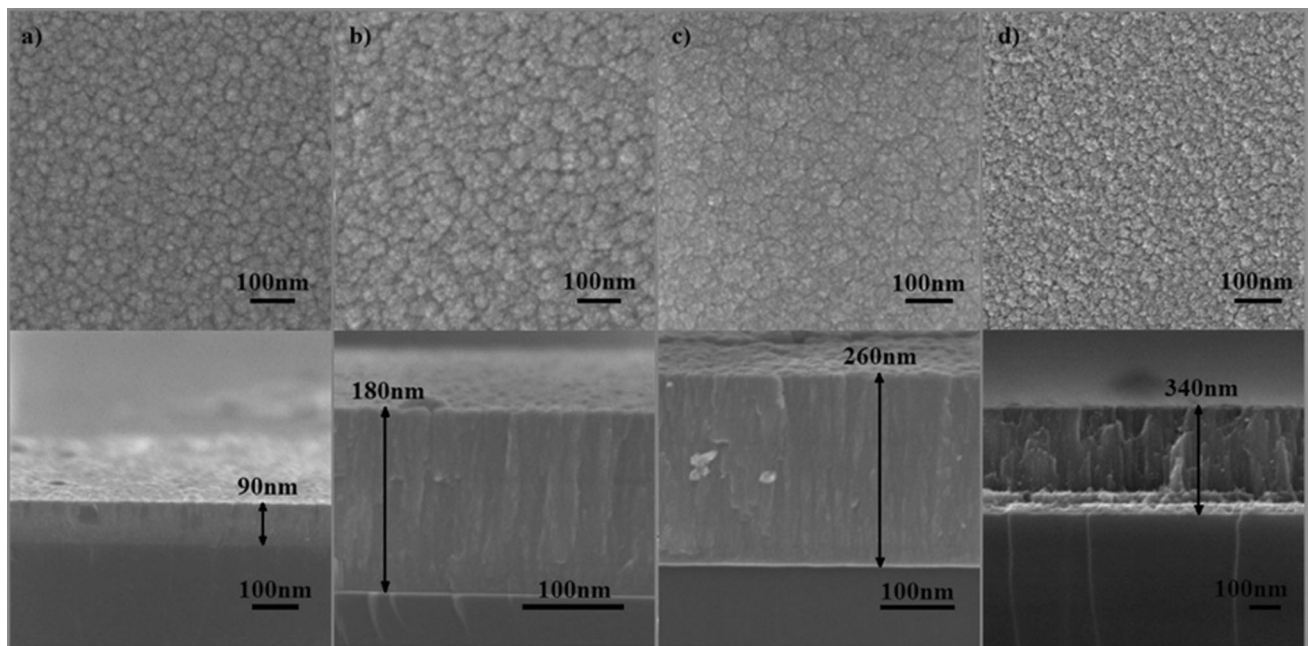


**Figure 2** SEM images (top view and cross-section) of as-deposited $MoO_x$ films **a** H1, **b** H2, **c** H3 and **d** H4.

increased from 90 to 180 nm, H2 from 180 to 280 nm, H3 from 260 to 450 nm and finally H4 from 340 to 570 nm. This change could be correlated with the change in interatomic distance of the molybdenum oxide; for example, the lattice constant of $b$ in $MoO_2$ is 4.859 Å, while in α-$MoO_3$ the $b$ parameter is 13.855 Å [25]. When $MoO_2$ transforms in $MoO_3$, an extra oxygen atom is incorporated for every molybdenum atom, and at the same time, a modification of the crystalline structure could occur. Considering the mass of the formula unit for $MoO_2$ y $MoO_3$ (127.92

and 143.96, respectively) and the corresponding densities (6.47 and 4.69 g/cm$^3$, respectively), it can be calculated that the volume (thickness) of $MoO_3$ is around 1.55 time of the original $MoO_2$ volume. We found even larger increments of the thickness probably because of the difference in the porosity of the films before and after annealing.

For the crystallographic studies of the thin films, XRD analysis was carried out. Figure 4a shows the XRD patterns for the as-deposited samples (H1–H4). The films in general shown the presence of α-$MoO_3$
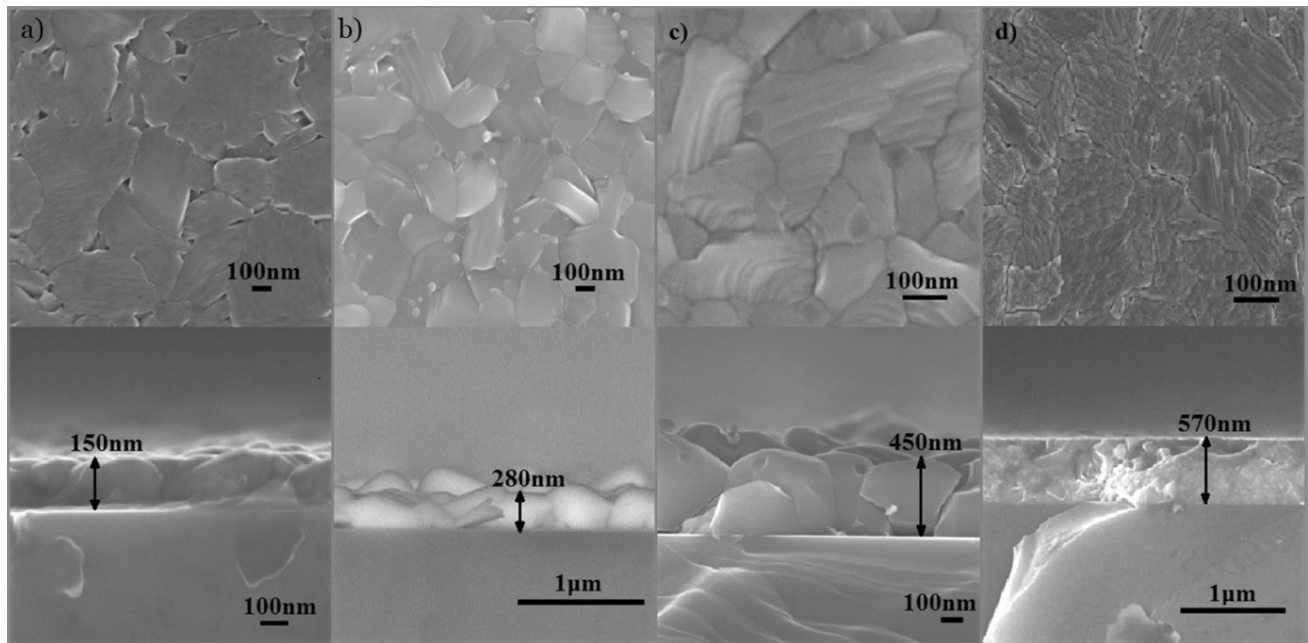
**Figure 3** SEM images (top view and cross-section) of annealed $MoO_x$ films **a** H1, **b** H2, **c** H3 and **d** H4.

(JCPD card number 03-065-2421), $\beta$-$MoO_2$ (card number 01-076-1807) and $\gamma$-$Mo_4O_{11}$ (card number 00-013-0142). This result also corroborates the estimation made earlier regarding the average density of the material deposited (presence of sub-oxide phases). The presence of the mixed phases $\alpha$-$MoO_3$, $\beta$-$MoO_2$ and $\gamma$-$Mo_4O_{11}$ could be due to the deficient oxygen content in the sputter chamber during the deposition of thin films. Presence of broad peaks could be correlated with the presence of small crystallites and amorphous nature of the as-deposited samples.

The role of annealing is quite significant from the XRD spectra. A considerable decrease/increase in the peaks intensity corresponding to the $MoO_2$/$MoO_3$ phases in annealed samples evidences the transformation of $\beta$-$MoO_2$ to $\alpha$-$MoO_3$. This can explain, at least in part, the increase in the thickness after annealing as explained above.

Previous works have reported the same kind of tendency, and the reason was found to be the excess of oxygen concentration in the sample [3]. Apart from that, some other studies were also carried out where the role of the partial pressure of oxygen was varied during the deposition and presence of various sub-oxide phases was demonstrated [35, 36]. It was shown that the quantity of oxygen present in the

chamber is a deciding factor in obtaining various sub-oxides.

Moreover, using the XRD spectra the size of the crystallites was also calculated using the Debye–Scherrer relation for the peaks corresponding to the $MoO_3$ phase [37].

$$\tau = \frac{K\lambda}{\beta \cos \theta}$$

where $\lambda$ is the wavelength of the X-ray used, $\beta$ is the full width at half maximum of diffraction intensity and $\theta$ is the diffraction angle. The crystallite size was increased from value of around 10 nm to a value of 45 nm because of the heat treatment and subsequent oxidation process.

After having the information regarding the topography, surface morphology and crystallographic structure, more details regarding the chemical composition were studied using the XPS. To avoid complexity, in Fig. 5 we show the XPS spectra of two specific samples H1 (thinnest) and H4 (thickest).

Figure 5 shows the XPS spectra of Mo 3d levels for the thin films. A doublet is observed due to the spin–orbit splitting of Mo 3d levels around at 232.0 and 227.9 eV giving rise to Mo $3d_{5/2}$ and Mo $3d_{3/2}$, respectively [38]. By deconvolution of the 3d band of molybdenum, it was found a higher concentration of $\beta$-$MoO_2$ of around 90% in all of the as-grown
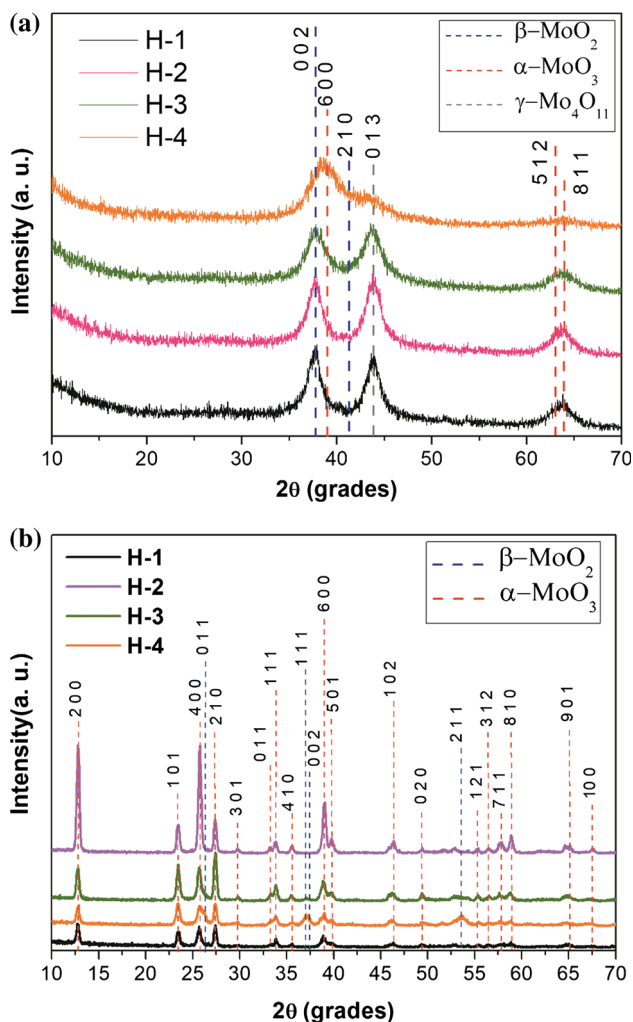
**Figure 4** **a** XRD profiles of as-deposited $MoO_x$ films showing the presence of three different kinds of oxidation states. **b** Shows the comparison of the XRD pattern for the annealed samples.



**Figure 5** Narrow scan Mo 3d XPS spectrum of as-deposited $MoO_x$ films **a** H1 and **b** H4.

samples. As expected, the predominance of the phase $\beta$-$MoO_2$ and the presence of other sub-phases such as $\alpha$-$MoO_3$ (3–4%) and $\gamma$-$Mo_4O_{11}$ (6 to 7%) is evident.

On the other hand, Fig. 6 shows the deconvolutions of the Mo 3d states corresponding to samples H1 and H4 after the thermal treatment. As expected from XRD analysis (Fig. 4), there is a predominance of $\alpha$-$MoO_3$ (around 80%) and a lesser content of $\gamma$-$Mo_4O_{11}$ phase (around 20%). However, in comparison with XRD, $MoO_2$ phase could not be observed for any sample. In conclusion, we have $MoO_x$ thin films with a greater concentration of $\beta$-$MoO_2$ before and $\alpha$-$MoO_3$ after the thermal treatment; the presence of the sub-stoichiometric $\gamma$-$Mo_4O_{11}$ can be seen in all cases. A significant change in the proportion of the molybdenum compounds after annealing would
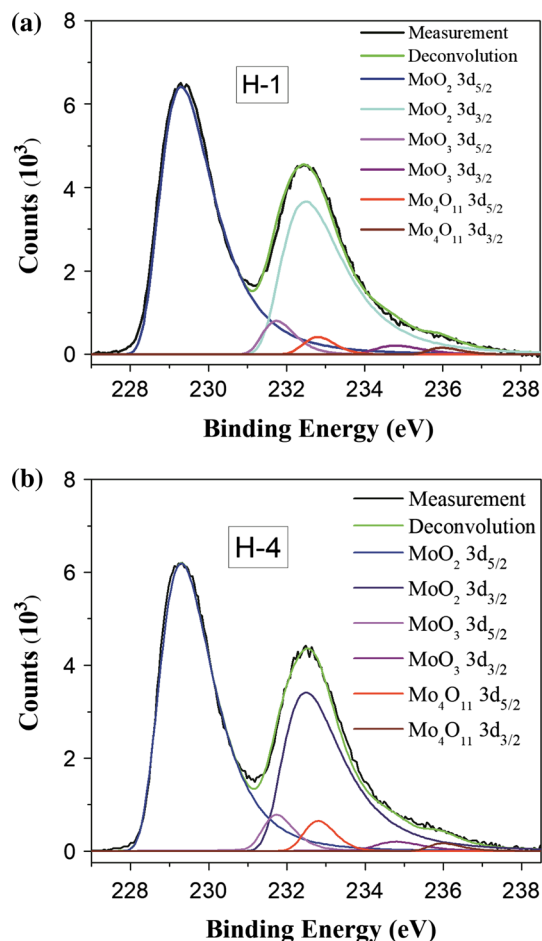
bring significant changes in the optoelectronic properties of the obtained films, which will be studied in the next section.

The optical transmission spectra of both as-deposited and annealed films are shown in Fig. 7. It has been shown that annealing in air strongly affects the optical transmittance of $MoO_x$ films. In the case of $MoO_x$ as-grown thin films, low transmission is attributed to the oxygen ion vacancies, which reduces the band gap and increases the free carrier concentration [3, 31, 39]. Increase in the optical transmittance after annealing could be due to the reduction in oxygen ion vacancies and due to the transformation of the partial oxidized thin film into nearly stoichiometric $\alpha$-$MoO_3$ films with a wide band gap and semiconductor behavior (Figs. 4 and 6).

From the solid band theory, the optical band gap ($Eg$) of the films was calculated from the optical
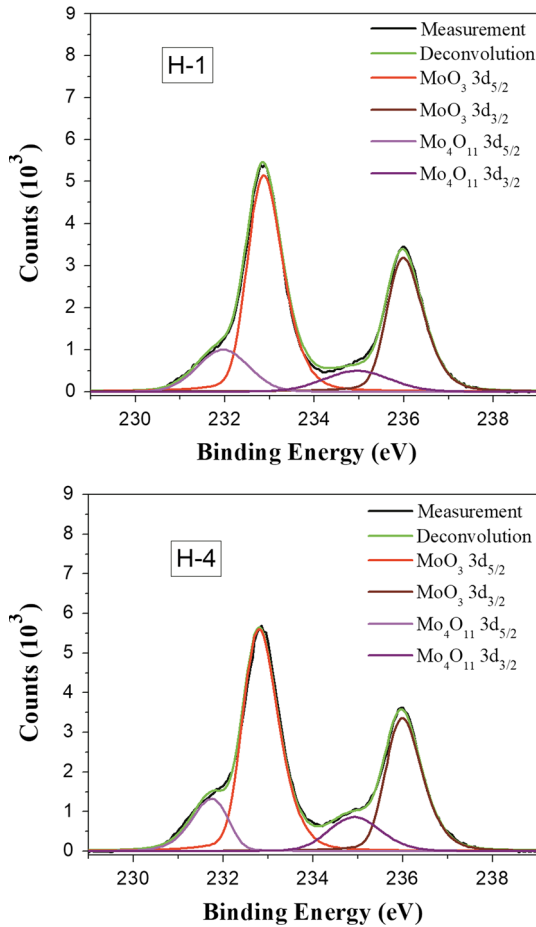
**Figure 6** Narrow scan Mo 3d XPS spectrum of annealed $MoO_x$ films annealed under air atmosphere at 400 °C for 60 min.

absorption coefficient using the Tauc relation [40]. The band gap values are illustrated in Table 1.

The optical band gaps computed from the Tauc relation are estimated to vary from almost 0.02 eV (H3 and H4—before annealing) to around 3.2–3.3 eV (H1 and H2—after heat treatment). The low band gap value of the films with higher thickness could be due to the formation of sub-stoichiometric phases ($MoO_2$, $Mo_4O_{11}$ and $MoO_3$). It is due to the fact that in the as-grown samples, oxygen vacancies create an excess of free carrier concentration, which could result in the generation of a semimetallic behavior in the thin films. [3]. Furthermore, band gap values of near around 3.5 eV have been reported earlier for amorphous and crystalline $MoO_3$ films [41]. Other groups [42, 43] have shown an increase in the band gap for stoichiometric thin films by means of DC magnetron sputtering and spray pyrolysis.

Control over the thickness (Figs. 2 and 3), oxidation state (Figs. 4, 5 and 6) and hence material type (semimetallic or semiconductor properties) of the films deposited in the present work could result in a structure which could be used in multiple applications.

As a final study, photoconductivity measurements were carried out. The aim of this analysis was to show the use of $MoO_x$ films developed in the present work for applications such as buffer layer or the passivation layer in solar cell and/or for the fabrication of selective contacts in the modern generation of solar cells. In general, it has been reported that a very thin layer of $MoO_3$ could act as a transparent hole-selective contact to n-type silicon [9], whereas once the stoichiometry is changed ($MoO_{3-x}$), it may be considered as a high work-function metal with a
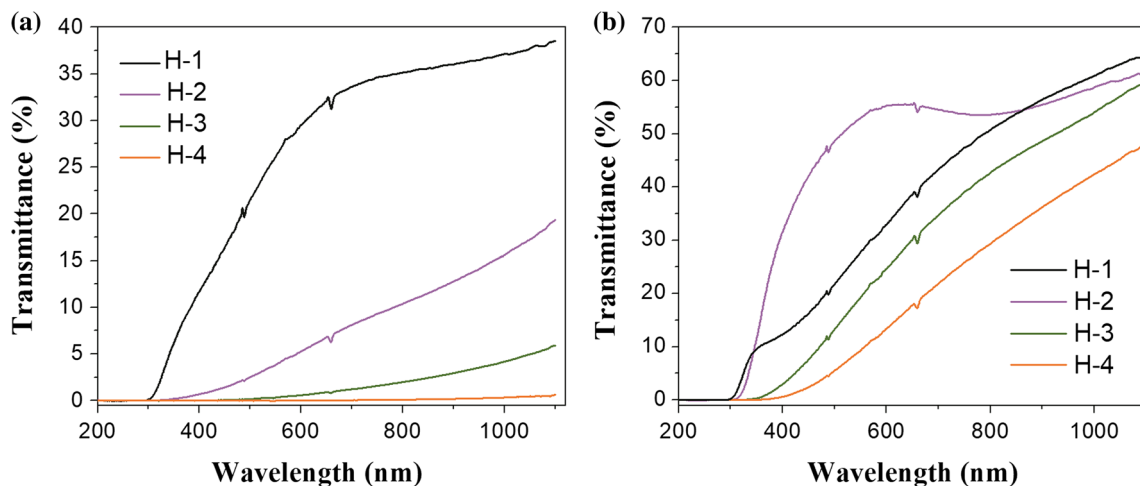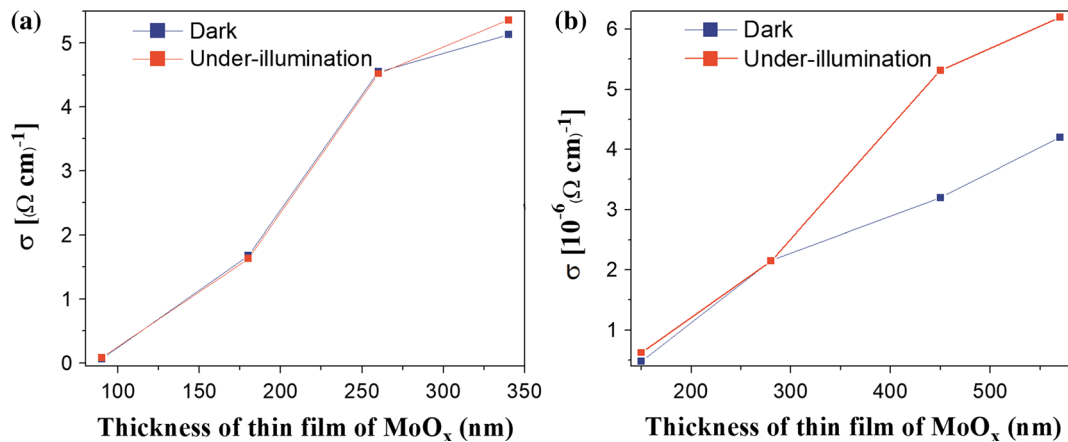


**Figure 7** Variation of optical transmittance of as-deposited (**a**) and annealed (**b**) $MoO_x$ films deposited on glass substrates.

**Table 1** Band gap values of the thin films of $MoO_x$ before and after heat treatment

| Samples | Band gap value (before; eV) | After heat treatment (eV) |
|---------|------------------------------|---------------------------|
| H-1 | 3.33 | 3.36 |
| H-2 | 1.25 | 3.28 |
| H-3 | 0.02 (semimetallic behavior) | 2.13 |
| H-4 | 0 (semimetallic behavior) | 1.56 |



**Figure 8** **a** Photoconductivity comparison of the as-deposited samples and **b** annealed $MoO_x$ films.

low density of states at the Fermi level originating from the tail of an oxygen vacancy [25]. For this reason, studies were carried out to find out the influence of these oxygen concentration variations on the optoelectronic properties of the material.

The photoconductivity of the four different films (as-deposited and annealed) is shown in Fig. 8. Figure 8a shows the relationship between the dark and under-illumination conductivity as in response to the different thickness (H1–H4) of the as-deposited samples. It could be noted that in this case, before the thermal treatment, $MoO_x$ films did not show any significant change in their electrical conductivity after being illuminated. Only a slight increase in electrical conductivity of sample H4 was observed. On the other hand, after annealing, the thinner samples (H1 and H2) again did not reveal any noteworthy changes in their optical conductivity after being illuminated. The reason could be due to their higher band gap and lower effective absorption in the visible region, whereas, after being illuminated, samples H3 and H4, shown 66 and 48%, respectively, increase in their electrical conductivity in Fig. 8b. In general, six orders of magnitude decrease in the conductivity (Y-axis) could be observed in the annealed samples in Fig. 8b (semiconductor phase behavior) as in

comparison with as-deposited samples in Fig. 8a (semimetallic phase behavior).

Hence, the deposition conditions (role of thickness and oxidation state) and investigation revealed in the work could present a good establishment for the development of $MoO_x$ thin films for a vast number of applications especially in the area of new generation solar cells (organic, perovskite, dye synthesized and inorganic solar cells) where the conductivity change under solar irradiation could be a vital parameter for understanding the final device properties.

## Conclusions

In the present work, we proposed a new kind of control over the growth technique and properties of $MoO_x$ films deposited using a simple and economic DC Cressington sputtering system. As well known, Mo has a higher tendency of being oxidized in the air, and hence, its relative properties (morphological and optoelectronic) could change a lot. Here, we demonstrated the growth of the Mo thin films keeping in account the oxidation occurring during the low vacuum deposition (without the addition of oxygen). By adjusting the deposition time, control over the thickness and hence sub-oxide states were

established. Using AFM and SEM, it was found that the thicker films were rougher; in addition, after the annealing, they attained a smaller grain size and a lower roughness than the thinnest films. XRD and XPS analysis shown that before the annealing, a mixture of crystalline phases: α-MoO$_3$, β-MoO$_2$, and γ-Mo$_4$O$_{11}$, with MoO$_2$ being predominant, was observed, whereas after annealing, MoO$_3$ was found to be in majority. Before the heat treatment, the thicker samples (H3 and H4) exhibit a metallic behavior (with no band gap), whereas H2 has a typical semiconductor behavior and H1 tends to have insulating features. After the heat treatment, samples H3 and H4 shown a typical semiconductor behavior, while samples H1 and H2 have an insulating character. The electrical conductivity of the samples tends to be higher in thicker samples, for both cases (before and after the annealing). Before annealing, the films did not show any photoconductivity effects, except perhaps a slight increase in the electrical conductivity that was observed in the H4 sample when illuminated; however, after the heat treatment, an appreciable effect of the illumination on the electrical conductivity of samples H3 and H4 is evident. Finally, work presented in this article provides a good basis for the control over the morphology and properties of MoO$_x$ thin films for various optoelectronic applications.

## References

[1] Granqvist CG (1995) Handbook of inorganic electrochromic materials. Elsevier, Amsterdam

[2] Hinokuma K, Kishimoto A, Kudo T (1994) Coloration dynamics of spin-coated MoO$_3$·nH$_2$O electrochromic films fabricated from peroxo-polymolybdate solution. J Electrochem Soc 141(4):876–879. https://doi.org/10.1149/1.2054850

[3] Subbarayudu S, Madhavi V, Uthanna S (2013) Growth of MoO3 Films by RF magnetron sputtering: studies on the structural, optical, and electrochromic properties. ISRN Condens Matter Phys 2013:806374

[4] Walia S, Balendhran S, Nili H, Zhuiykov S, Rosengarten G, Wang QH, Bhaskaran M, Sriram S, Strano MS, Kalantarzadeh K (2013) Transition metal oxides—thermoelectric properties. Prog Mater Sci 58:1443–1489

[5] Scarminio J, Lourenco A, Gorenstein A (1997) Electrochromism and photochromism in amorphous molybdenum oxide films. Thin Solid Films 302:66–70

[6] Prasad AK, Kubinski DJ, Gouma PI (2003) Comparison of sol-gel and ion beam deposited MoO$_3$ thin film gas sensors for selective ammonia detection. Sens Actuators B 93:25–30

[7] Gretener C, Perrenouda J, Kranza L et al (2013) Development of MoO$_x$ thin films as back contact buffer for CdTe solar cells in substrate configuration. Thin Solid Films 535:193–197

[8] Tong J, Wan Y, Cui J, Lim S, Song N, Lennon A (2017) Solution-processed molybdenum oxide for hole-selective contacts on crystalline silicon solar cells. Appl Surf Sci 423:139–146

[9] Battaglia C, Yin X, Zheng M, Sharp ID, Chen T, McDonnell S, Azcatl A, Carraro C, Ma B, Maboudian R, Wallace RM, Javey A (2014) Hole selective MoO$_x$ contact for silicon solar cells. Nano Lett 14(2):967–971

[10] Bullock J, Cuevas A, Allen T, Battaglia C (2014) Molybdenum oxide MoO$_x$: a versatile hole contact for silicon solar cells. Appl Phys Lett 105:232109

[11] Gerling LG, Mahato S, Voz C, Alcubilla R, Puigdollers J (2015) Characterization of transition metal oxide/silicon heterojunctions for solar cell applications. Appl Sci 5:695–705

[12] Wrfel P (2005) Physics of solar cells, 1st edn. Wiley, Weinheim, pp 113–114

[13] Bullock J, Yan D, Cuevas A, Wan Y, Samundsett C (2015) n- and p-type silicon solar cells with molybdenum oxide hole contacts. Energy Proc. 77:446–450

[14] Alsaif MM et al (2014) Tunable plasmon resonances in two-dimensional molybdenum oxide nano flakes. Adv Mater 26:3931–3937

[15] Diaz-Droguett DE, Zúñiga A, Solorzano G, Fuenzalida VM (2012) Electron beam-induced structural transformations of MoO$_3$ and MoO$_{32x}$ crystalline nanostructures. J Nanopart Res 14:1–9

[16] Fleisch TH, Zajact GW, Schreiner JO, Mains GJ (1986) An XPS study of the UV photoreduction of transition and noble metal oxides. Appl Surf Sci 26:488–497

[17] Grasselli RK (1999) Advances and future trends in selective oxidation and ammoxidation catalysis. Catal Today 49:141–153

[18] Haber J, Lalik E (1997) Catalytic properties of MoO₃ revisited. Catal Today 33:119–137

[19] Alsaif Manal M Y A et al (2016) High-performance field effect transistors using electronic inks of 2D molybdenum oxide nanoflakes. Adv Funct Mater 26:91–100

[20] Chen CZ, Li Y, Tang XD (2016) Evidence of oxygen vacancy and possible intermediate gap state in layered α - MoO₃ single-crystal nanobelts. Phys B Condens Matter 481:192–196

[21] Meyer J, Hamwi S, Kroger M, Kowalsky W, Riedl T, Kahn A (2012) Transition metal oxides for organic electronics: energetics, device physics and applications. Adv Mater 24(40):5408–5427

[22] McDonnell S, Azcatl A, Addou R, Gong C, Battaglia C, Chuang S, Cho K, Javey A, Wallace RM (2014) Hole contacts on transition metal dichalcogenides: interface chemistry and band alignments. ACS Nano 8(6):6265–6272

[23] Chuang S, Battaglia C, Azcatl A, McDonnell S, Kang JS, Yin X, Tosun M, Kapadia R, Fang H, Wallace RM, Javey A (2014) MoS₂ p-type transistors and diodes enabled by high work function MoOₓ contacts. Nano Lett 14(3):1337–1342

[24] Greiner MT, Chai L, Helander MG, Tang W-M, Lu Z-H (2012) Transition metal oxide work functions: the influence of cation oxidation state and oxygen vacancies. Adv Funct Mater 22(21):4557–4568

[25] de Castro IA (2017) Molybdenum oxides—from fundamentals to functionality. Adv Mater Adv Mater 29:1701619

[26] Sian TS, Reddy GB (2005) Stoichiometric amorphous MoO₃ films: a route to high performance electrochromic devices. J Appl Phys 98:026104

[27] Sivakumar R, Gopalakrishnan R, Jayachandran M, Sanjeeviraja C (2007) Characterization on electron beam evaporated -MoO₃ thin films by the influence of substrate temperature. Curr Appl Phys 7:51–59

[28] Ramana CV, Julien CM (2006) Chemical and electrochemical properties of molybdenumoxide thin films prepared by reactive pulsed-laser assisted deposition. Chem Phys Lett 428:114–118

[29] Nirupama V, Uthanna S (2016) Investigations on morphological and electrical studies of sputtered MoO₃ films. J Mater Sci Mater Electron 27:3668–3674

[30] Itoh T, Matsubara I, Shin W, Izu N, Nishibori M (2008) Preparation of layered organic-inorganic nanohybrid thin films of molybdenum trioxide with polyaniline derivatives for aldehyde gases sensors of several tens ppb level. Sens Actuators B 128:512–520

[31] Balaji M, Chandrasekaran J, Raja M, Rajesh S (2016) Structural, optical and electrical properties of Ru doped MoO₃ thin films and its P–N diode application by JNS pyrolysis technique. J Mater Sci Mater Electron 27:11646–11658

[32] Hsu CS, Chan C-C, Huang H-T, Peng C-H, Hsu W-C (2008) Electrochromic properties of nanocrystalline MoO₃ thin films. Thin Solid Films 516:4839–4844

[33] Chang W-C, Qi X, Kuo J-C, Lee S-C, Ng S-K, Chen D (2011) Post-deposition annealing control of phase and texture for the sputtered MoO₃ films. CrystEngComm 13:5125–5132

[34] Hussain S, Shehzad MA, Vikraman D, Khan MF, Singh J, Choi D-C, Seo Y, Eom J, Lee W-G, Jung J (2016) Synthesis and characterization of large-area and continuous MoS₂ atomic layers by RF magnetron sputtering. Nanoscale 8:4340–4347

[35] Subbarayudu S, Madhavi V, Uthanna S (2013) Post-deposition annealing controlled structural and optical properties of RF magnetron sputtered MoO₃ films. Adv Mater Lett 4:637–642

[36] Nirupama V, Gunasekhar KR, Sreedhar B, Uthanna S (2010) Effect of oxygen partial pressure on the structural and optical properties of dc reactive magnetron sputtered molybdenum oxide films. Curr Appl Phys 10:272–278

[37] Cullity BD (1978) Elements of X-Ray diffraction, 2nd edn. Addison Wesley, London

[38] Diaz-Droguett DE, Fuenzalida VM, Diaz-Espinoza MS, Solorzano G (2008) Electron beam effects on amorphous molybdenum oxide nanostructures grown by condensation in hydrogen. J Mater Sci 43:591–596. https://doi.org/10.1007/s10853-007-1602-1

[39] Sabhapathi VK, Hussain OM, Reddy PS et al (1995) Optical absorption studies in molybdenum trioxide thin films. Phys Status Solidi A 148:167–173

[40] Tauc J (1974) Amorphous and liquid semiconductor. Plenum Press, New York

[41] Okumu J, Koerfer F, Salinga C, Pedersen TP, Wuttig M (2006) Gasochromic switching of reactively sputtered molybdenumoxide films: a correlation between film properties and deposition pressure. Thin Solid Films 515:1327–1333

[42] Mohamed SH, Venkataraj S (2007) Thermal stability of amorphous molybdenum trioxide films prepared at different oxygen partial pressures by reactive DC magnetron sputtering. Vacuum 81:636–643

[43] Boudaoud L, Benramdane N, Desfeux R, Khelifa B, Mathieu C (2006) Structural and optical properties of MoO₃ and V₂O₅ thin films prepared by spray pyrolysis. Catal Today 113:230–234